Antibacterial properties of laser-encapsulated titanium oxide nanotubes decorated with nanosilver and covered with chitosan/Eudragit polymers

Łukasz Pawłowski [a,*], Jakub Wawrzyniak [b], Adrianna Banach-Kopeć [c], Bartłomiej Michał Cieślik [d], Kacper Jurak [e], Jakub Karczewski [f], Robert Tylingo [c], Katarzyna Siuzdak [b], Andrzej Zieliński [a]

[a] Institute of Manufacturing and Materials Technology, Faculty of Mechanical Engineering and Ship Technology, Gdańsk University of Technology, Narutowicza 11/12, 80-233 Gdańsk, Poland
[b] Center for Plasma and Laser Engineering, The Szewalski Institute of Fluid-Flow Machinery, Polish Academy of Sciences, Fiszera 14, 80-231 Gdańsk, Poland
[c] Department of Chemistry, Technology and Biotechnology of Food, Faculty of Chemistry, Gdańsk University of Technology, Narutowicza 11/12, 80-233 Gdańsk, Poland
[d] Department of Analytical Chemistry, Faculty of Chemistry, Gdańsk University of Technology, Narutowicza 11/12, 80-233 Gdańsk, Poland
[e] Department of Electrochemistry, Corrosion and Materials Engineering, Faculty of Chemistry, Gdańsk University of Technology, Narutowicza 11/12, 80-233 Gdańsk. Poland
[f] Institute of Nanotechnology and Materials Engineering, Faculty of Applied Physics and Mathematics, Gdańsk University of Technology, Narutowicza 11/12, 80-233 Gdańsk, Poland

ARTICLE INFO

ABSTRACT

To provide antibacterial properties, the titanium samples were subjected to electrochemical oxidation in the fluoride-containing diethylene glycol-based electrolyte to create a titanium oxide nanotubular surface. Afterward, the surface was covered by sputtering with silver 5 nm film, and the tops of the nanotubes were capped using laser treatment, resulting in an appearance of silver nanoparticles (AgNPs) of around 30 nm in diameter on such a modified surface. To ensure a controlled release of the bactericidal substance, the samples were additionally coated with a pH-sensitive chitosan/Eudragit 100 coating, also exhibiting bactericidal properties. The modified titanium samples were characterized using SEM, EDS, AFM, Raman, and XPS techniques. The wettability, corrosion properties, adhesion of the coating to the substrate, the release of AgNPs into solutions simulating body fluids at different pH, and antibacterial properties were further investigated. The obtained composite coatings were hydrophilic, adjacent to the surface, and corrosion-resistant. An increase in the amount of silver released as ions or metallic particles into a simulated body fluid solution at acidic pH was observed for modified samples with the biopolymer coating after three days of exposure avoiding burst effect. The proposed modification was effective against both Gram-positive and Gram-negative bacteria.

1. Introduction

Surface modification of long-term metallic implant materials, especially titanium and its alloys, remains the focus of numerous studies aimed at improving the bonding of the implant to surrounding tissues without adverse reactions such as corrosion or bacterial infections [1]. For instance, mechanical treatment of implant surfaces by sandblasting, dry or wet grinding, or polishing modifies the surface roughness of these materials, which translates into their physicochemical and biological properties [2]. One of the inquisitive examples of modification of titanium implants, still under investigation, is the fabrication of nanotube-like oxide layers. By electrochemical oxidation, usually in the presence of fluoride ions in an electrolyte into which a titanium sample is introduced, a nanotube oxide layer can be formed. By appropriate selection of process parameters such as voltage, time, temperature, the concentration of electrolyte components it is possible to control the morphology of produced structures [3,4].

Due to their porosity, large specific surface area providing a barrier to protect the implant from the aggressive external environment, and biocompatibility of titanium oxide nanotubes, they can enhance adhesion and proliferation of bone-forming cells [5]. Meanwhile, such structures will promote the adhesion of bacterial cells, which can result

---

* Corresponding author.
E-mail address: lukasz.pawlowski@pg.edu.pl (Ł. Pawłowski).

in biofilm formation and local inflammation, which in extreme cases may make the implant removal necessary [6]. Nanotubes by themselves do not exhibit a strong antibacterial effect, hence it is necessary to provide these structures with such properties through additional modification [7]. Frequently, nanotube structures act as reservoirs of a bactericidal active substance [8]. There are many examples in the literature of the incorporation of therapeutic substances into oxide nanotube layers such as gentamicin [9], vancomycin [10], tetracycline [11], or antibacterial peptide [12]. The therapeutic substance is usually introduced into the nanotubes by physical adsorption, immersion in solution, or hydrothermal treatment [6]. The deposition of antimicrobial metallic nanoparticles on nanotube oxide layers is also practiced and, most often, silver nanoparticles (AgNPs) are incorporated [13]. The nanotube oxide layer can be decorated with silver nanoparticles by silver salt reduction, sputtering, sonochemical synthesis, laser treatment, microwave irradiation, or electrodeposition methods (cyclic voltammetry, chronoamperometry) [14].

The antibacterial mechanism of silver is not fully explained but several actions have been proposed. The antimicrobial activity of AgNPs is based not only on the release of silver ions but also on the penetration of bacterial cells and their annihilation at sufficiently small particle sizes [15]. However, there is often a lack of control over the release of the bactericidal substance into the peri-implant tissues and the concentration of the active substance can reach toxic levels. It is particularly important to limit the burst release effect, which is the release of a large dose of the drug in a short time after the implant is introduced into the human body environment [16]. To mitigate this phenomenon, the pH-related coatings with nanosilver can be applied as, e.g., chitosan [17–20], some acrylates like Eudragit [21], or by some other compounds like poly(4-vinylpyridine) (P4VP) [22–24]. The nanotubes with the introduced active substance can be also covered with some smart biopolymer coatings that degrade under specific conditions releasing the drug [8].

The laser treatment was also used to modify the titanium surface, but rarely for nanotubular oxide layers. In particular, high-power laser irradiation was shown as a promising treatment for titanium dental implant surfaces [25]; the surface irradiation followed the previous immersion in Ca nitrate solution resulted in creating a modified layer with oxygen and calcium presence [26]. Pulse laser ablation of titanium surface in n-heptane formed a layer containing the titanium carbide which substantially decreased the friction coefficient and increased the hardness, not influencing the corrosion rate in Hank's solution [27]. Similar effects were observed after physical vapor deposition (PVD) of carbon film on titanium surface followed by the femtosecond laser treatment [28]. The superhydrophilic surfaces of high stability were produced by femtosecond laser followed by NaOH hydrothermal treatment [29].

This paper presents a promising type of modification of nanotube oxide layers fabricated on closed titania nanotubes, which involves two-step decoration with silver nanoparticles by sputtering followed by laser annealing. Subsequently, encapsulated nanotubes with silver species on the top were coated by electrophoretic method with chitosan/Eudragit 100 (chit/EE100) belonging to smart biopolymers biodegradable with decreasing pH of an environment and already investigated [30]. The novelty of the presented method lies in the unique approach to fabrication of the antibacterial composite, which protects against bacterial adhesion and local tissue inflammation. In this work, the system was enriched in AgNPs by laser treatment rather than using commercially available nanosilver powder, which greatly reduced the problem of their agglomeration occurring in previous studies [21].

The morphology, roughness, wettability, chemical composition, corrosion resistance, adhesion of the coating to the substrate, release profiles of AgNPs, and antimicrobial activity of the proposed nanotube oxide layer modifications were investigated.

2. Experimental section

2.1. Sample preparation

The titania nanotubes serving as a substrate material were synthesized via electrochemical oxidation of the titanium foil (99.7%) in the two-electrode system. The foil 0.127 mm thick (Strem Chemicals, UK) was cut into 35×25 mm pieces and degreased ultrasonically in acetone, ethanol, and deionized water for 10 min in each medium. After air drying, the foil was submerged in the diethylene glycol-based electrolyte containing 7.0 wt% deionized water, 0.5 wt% HF, and 0.3 wt% NH_4F, which was kept at a constant temperature of 40 °C. The foil acted as an anode, whereas platinum mesh was used as a cathode. The anodization potential was controlled by in-house built hardware and increased at the rate of 0.1 V/s up to 40 V, then kept for 2 h, and decreased at the same rate. Process parameters were chosen according to previous studies [31]. After the process, the samples were rinsed with distilled water and submerged in ethanol for around 1 h which was followed by thermal treatment in a furnace (Nabertherm, Germany) at 450 °C for 2 h. The substrate prepared in such a way was considered as a reference sample (Sample I). A further modification was done by sputtering (Q150T S, Quorum Technologies Ltd., UK) about 5 nm thick silver layer. Subsequently, the samples were placed on the motorized table (SmarAct, Germany) in a vacuum chamber (10^{-8} bar; Pfeiffer, Germany) and irradiated with the Nd: YAG pulsed laser equipped with a 3rd harmonics generator (Quantel Q-Smart 850, Lumibird, France) with 30 mJ/cm^2 laser pulses (Sample II). The final type of modification was the coverage of laser-modified nanotubes by deposition of the chit/EE100 coating using an electrophoretic method (Sample III). The deposition was performed with the protocol described previously [30]. In brief, the biopolymer suspension was prepared by introducing 0.1 g of chitosan (high molecular weight, purity >99%, degree of deacetylation >75%, Sigma-Aldrich, USA) and 0.25 g of Eudragit E 100 (molecular weight ~ 47 kDa, purity 99.9%, Evonik Industries, Germany) into 100 mL of 1% (v/v) aqueous acetic acid (99.9%; these and other chemicals delivered by the Avantor Performance Materials, Poland) solution and magnetic stirring (MS-H-Pro+, Dragon Lab, Poland) for 24 h at room temperature. The coatings were electrophoretically deposited in a two-electrode system. The cathode was a titanium foil with titanium dioxide nanotubes on the surface after laser treatment and sputtering of a silver layer, while the anode was a platinum mesh electrode. The distance between the electrodes was kept constant at approximately 10 mm. Coating deposition was conducted at a voltage of 10 V (DC power source MCP/SPN110-01C, Shanghai MCP Corp., China) for 1 min at room temperature. Following deposition, samples were washed with distilled water and allowed to dry in ambient air for 24 h.

2.2. Sample characterization

The scanning electron microscopy (JSM-7800 F, JEOL, Japan) was used to study the morphology of the modified titanium foils. An energy-dispersive X-ray spectroscopy module (EDS, Edax Inc., USA) enabled qualitative analysis of the chemical composition of the samples studied. For better SEM imaging, the biopolymer coated sample was additionally sputtered with a 10 nm thick chromium layer using a DC magnetron sputtering system (Q150T ES, Quorum Technologies Ltd., UK).

The surface roughness of the materials studied was determined using atomic force microscopy (NaniteAFM, Nanosurf, Switzerland). The measurement was performed with a non-contact mode at a force of 55 mN on an area of 50×50 μm. From each of the three measurements, the value of the parameter Sa (the arithmetic average deviation) was determined, which allowed describing the roughness of the tested surface.

The thickness of the chit/EE100 coating was measured using an FMP10-20 dual-band coating thickness meter (SN100146594, Helmut Fischer GmbH, Germany), and 10 measurements were taken, and the

average value was determined.

Surface wettability was investigated by the falling drop method using a goniometer (Attention Theta Life, Biolin Scientific, UK) at room temperature. The contact angle value for each sample was determined from five droplets of 2 μL of distilled water. The readings of the measuring instrument were taken 10 s after the droplet.

The Raman spectra were obtained by Renishaw inVia Raman microscope (Renishaw, UK) equipped with 514 nm laser using × 50 objective. The X-ray photoelectron spectra (XPS) were obtained from the sample via Escalab 250Xi (ThermoFisher Scientific, USA) calibrated for adventitious C_{1s} (284.6 eV) using Al Kα anode. The data analysis was performed by using Avantage software provided by the manufacturer.

A potentiodynamic method was implemented to determine the corrosion behavior of the tested samples. A three-electrode system, immersed in a simulated body fluid solution (SBF, 37 °C, chemical composition according to [19]), consisting of a sample as the working electrode, calomel and platinum electrodes as the reference electrode and a counter electrode, respectively, was used and connected to a potentiostat (Atlas 0531, Atlas Sollich, Poland). The samples were placed in the SBF for 1 h and the open circuit potential (OCP) values were recorded. Corrosion curves were determined for a potential range of −1/1 V at a potential rate of 1 mV/s. The corrosion potential (E_{corr}) and corrosion current density (j_{corr}) were assessed with the Tafel extrapolation method.

The linear voltammogram (for sample III) was obtained using the same circuit as above, in a three-electrode system (Metrohm Autolab PGStat 302 N, Netherlands). The sample acted as a working electrode, while Ag/AgCl/0.1 M KCl and platinum mesh were used as a reference and counter electrode, respectively. The sweeps were done from −0.8 to +1.0 V at the 1 mV/s rate.

The adhesion of the chit/EE100 coating to the closed titanium oxide nanotubular surface with AgNPs was investigated using a scratch test (NanoTest Vantage, Micro Materials, UK). Increasing the load in the range of 0–120 mN with a load rate of 1.3 mN/s, 10 scratches of 500 μm length each were made in the coating. For each scratch, the force causing complete delamination of the coating from the substrate was determined based on the observed rapid change in frictional force versus normal force and observations made using a light microscope (BX51, Olympus, Germany).

The release rate of silver into the same SBF solution at different pH was calculated using a microwave plasma atomic emission spectrometer (4210 MP-AES, Agilent, CA, USA). Samples containing silver nanoparticles were immersed in 50 mL of SBF solutions at different pH (3 and 7) for one day at 39 °C (to simulate inflammation), after which time they were transferred to a new 50 mL of the SBF solution. The procedure was repeated over three days. The pH of the SBF solution was corrected by the addition of 30% HCl. Measurements were conducted in neutral pH as well as in acidic pH at elevated temperatures to simulate the onset of local inflammation of peri-implant tissues [32,33]. The calibration solution used was ICP grade. Four repetitions and two separate procedures were performed at different wavelengths (328.06 nm and 338.28 nm) for different silver contents. Uncertainties were reported as the combined standard uncertainty (CSU) for all eight measurements that were based on the calibration solution.

The antimicrobial activity of the tested materials was evaluated using the standard ASTM E2149 method, with slight modification. The following bacterial strains were used for evaluation: *Escherichia coli* K-12 PCM 2560 (NCTC 10538) and *Staphylococcus aureus* PCM 2054 (ATCC 25923) from the Polish Collection of Microorganisms, Ludwik Hirszfeld Institute of Immunology and Experimental Therapy of the Polish Academy of Sciences (Wrocław, Poland). The strains that were deep-frozen stored in CrioBanks were first subcultured to tryptic soy broth (Sigma-Aldrich, Saint Louis, MO, USA) and incubated at 37 °C for 24 h. The bacterial suspension was diluted in phosphate buffer saline (pH 7.2) by measuring the absorbance at 600 nm (optical density 0.08 ÷ 0.1) to obtain a viable count of approximately 1.5×10^7 to 5×10^7 colony-

forming units per mL (CFU/mL). Samples I, II, and III and PE film (negative control without antimicrobial properties) with a side length of 5 cm were sterilized under UV light for 30 min on both sides of the materials. Subsequently, 0.2 mL of previously prepared suspensions of the tested bacterial strain were applied to each of the thus prepared materials. Additionally, a proper contact between the tested material and the strain of bacteria was ensured on the surface of 16 cm². For this purpose, the surface was covered with sterile PE films with a side length of 4 cm. After 24 h incubation at 37 °C (Heidolph 1000 Incubator, Merck Sp. z o.o., Warsaw, Poland), the materials were transferred into 10 mL of PBS solution and intensively vortexed for 25 s. Then, 10-fold serial dilutions in peptone water ($10^0 \div 10^8$) were plated on tryptic soy agar (TSA) medium by flooding, and the plates were incubated at 37 °C for 24 h. After incubation, the bacterial colonies that grew on the Petri dishes and ranged between 30 ÷ 300 CFU were counted according to the equation:

$$V_c = N \times D,$$

where V_c is the bacteria concentration (CFU/mL), N is the average value (CFU) from Petri dishes, and D represents the dilution factor from the plates counted. Antimicrobial activity was calculated by the formula:

$$R = log(B/C),$$

where B is the average of the number of viable cells on the tested sample after 24 h incubation at 37 °C (CFU/mL), C is the average of the number of viable cells on the control sample after the same incubation time at 37 °C (CFU/mL), R represents a percentage reduction of bacteria on a logarithmic scale. A reduction of 90%, 99%, and 99.9% corresponds to an R-value of 1, 2, and 3, respectively.

3. Results and discussion

Fig. 1 shows the morphology of samples I (Fig. 1a, b, and c), II (Fig. 1a', b', and c'), and III (Fig. 1d and d'). The titanium oxide nanotubes had diameters of around 206 ± 23 nm and exhibited distinct lateral spacing of about 125 ± 28 nm. After the laser treatment, the width of the nanotubes increased to 230 ± 19 nm, whereas the distance between them changed to 124 ± 39 nm. A slight change in the spatial geometry between Samples I and II could be expected, as the nanotubes were wider at the bottom and the melting of the nanotubes induced by the laser irradiation decreased their length by around 30%. Nevertheless, the formation of silver nanoparticles on the enclosed nanotubes is observed, as shown in Fig. 1b'. Most nanoparticles are of the order of 27 ± 7 nm except for bigger agglomerates on top of the nanotubes.

The chit/EE100 coating deposited by the electrophoretic method completely covered the modified nanotube substrate. Images obtained at higher magnifications revealed the porous morphology of the biopolymer coating. Like in previous studies [21,30], at lower values of voltage and deposition time, traces of hydrogen bubbles formed by electrolysis of water contained in the suspension were less visible, resulting in a relatively smoother coating.

The surface topographies of investigated samples determined by atomic force microscopy are depicted in Fig. 2a. From the obtained maps, it was found that the laser modification of the nanotube oxide layer contributed to the increase in surface roughness. Deposition of the biopolymer coating resulted in filling in any surface irregularities and obtaining a smooth surface of the sample. These observations coincide with the calculated mean values of the Sa parameter. There is an increase in the Sa value of the sample after laser treatment compared to the reference sample and a decrease in the Sa value after deposition of the biopolymer coating on sample II. The surface roughness of implant materials is one of the key factors determining the process of cell adhesion and proliferation, and thus the proper bonding of the implant with the surrounding tissues [34]. It has been reported that increased surface roughness contributes to better cell adhesion and primary
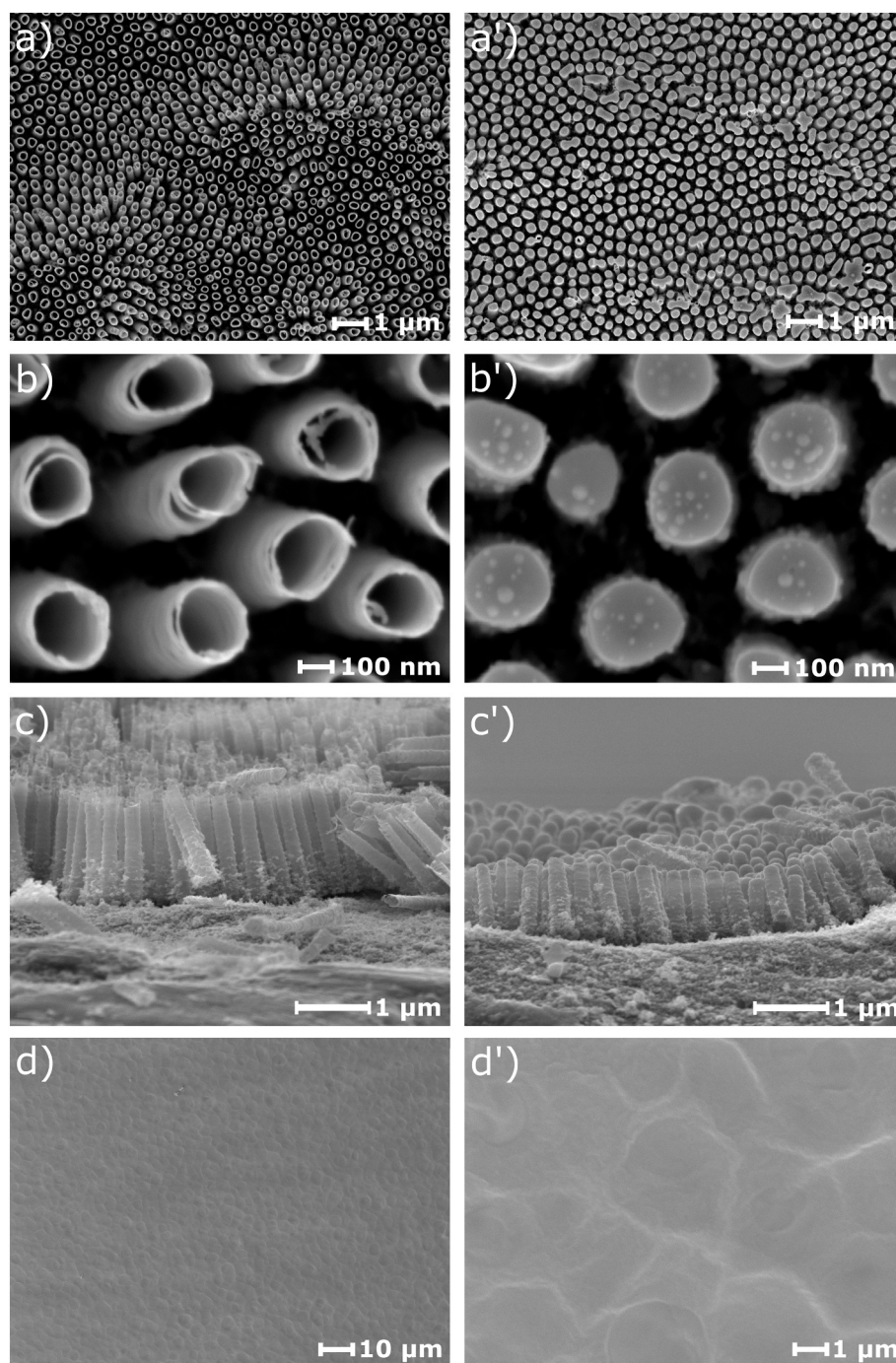
Fig. 1. Morphology and the cross-sections: (a), (b), (c) of the as-prepared TiO₂ nanotube oxide layer (Sample I); (a'), (b'), (c') of the laser modified nanotube layer with fabricated AgNPs (Sample II); and (d), (d') of the chit/EE100 coating on a modified oxide nanotube layer (Sample III).

stabilization of the implant; however, it may also contribute to facilitated bacterial cell adhesion increasing the risk of implant-related bacterial infections, hence such systems are enriched with antibacterial agents [35].

The thickness of the chit/EE100 coating was 2.67 ± 0.53 μm and this value is similar to the results obtained in previous studies [21].

The wettability measurement results of the tested samples are shown in Fig. 2b. All samples have hydrophilic surfaces (contact angle below 90°), which is essential for long-term implant applications [36]. The reference sample with the nanotube oxide layer shows the highest wettability, the most likely because the droplet has floated into the interstices between the fabricated nanotubes or flowed into the nanotubes.

The applied laser treatment reduced this phenomenon by encapsulating the nanotubes. Additionally, the produced nanoparticles also contribute to the increase in measured contact angle [37]. Eudragit E 100 exhibited hydrophobic properties [38], hence after deposition of the coating based on this biopolymer, a significant increase in the contact angle value could be observed, but still not exceeding 90°. The contact angle (θ) value here observed is similar to that obtained in previous studies [21,35].

Based on the analysis of the XPS spectra of sample II, the chemical composition of the silver nanoparticles was determined (Fig. 2c). Peaks located at 367.7 and 373.7 eV indicate dominant AgO content, whereas much smaller signals at 368.4 and 374.4 eV can be attributed to metallic
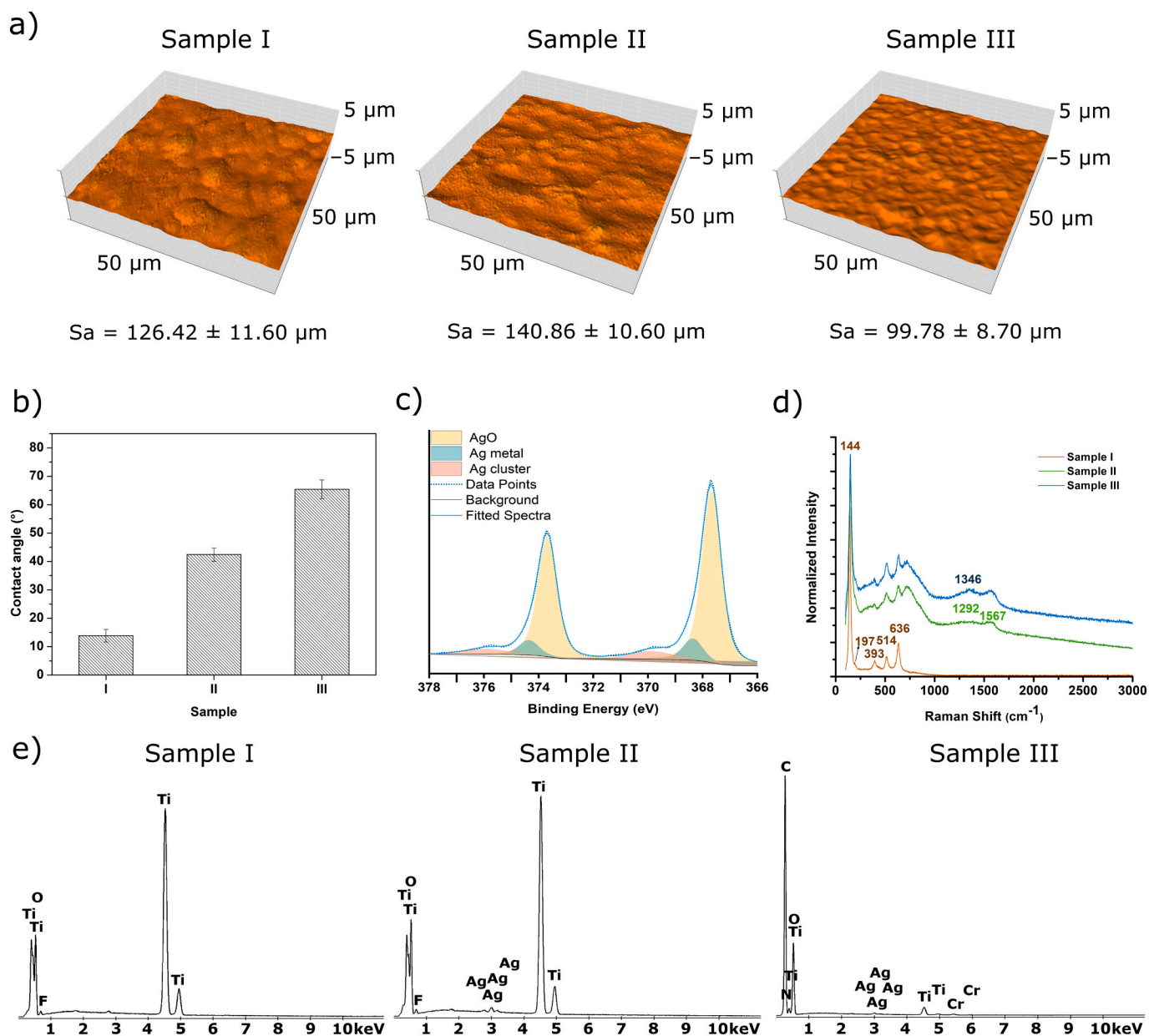
Fig. 2. (a) AFM maps with the measured value of Sa, (b) results of the wettability test, (c) the XPS spectra of sample II in the energy range of silver, (d) the Raman spectra, and (e) EDS analysis results of the studied samples.

Ag. The small, wide humps located at 369.8 and 375.9 eV come from plasmonic silver nanoclusters, and their width can be associated with the large size distribution of the nanoparticles [39–41]. The XPS did not, however, detect any silver contents in sample III due to the too high thickness of the deposited polymer layer.

These findings are supported by the Raman measurements for all three prepared samples (Fig. 2d). In all cases, the maxima at 144 ($E_{g(1)}$), 197 ($E_{g(2)}$), 393 (B_{1g}), 514 (B_{1g}), and 636 ($E_{g(3)}$) cm^{-1} are visible, characteristic for the crystalline anatase phase [42]. In the samples with a sputtered silver layer, a wide background typical of metals appears, confirming the presence of metallic Ag, though some of the wide backgrounds below 1000 cm^{-1} may be attributed to the laser-treatment induced amorphous TiO$_2$ as well. The peaks at 1292 and 1567 cm^{-1} confirm the presence of silver (II) oxide, and the heightened spectrum around 1364 cm^{-1} can be identified as a vibrational mode of C=O from the polymer coating [43–45].

The results of EDS analysis of titanium films after electrochemical oxidation, the oxidation followed by sputtering and laser treatment, and the foil after all these treatments and subsequent electrophoretic deposition of biopolymer coating are shown in Fig. 2e. Peaks from the substrate material (Ti and O) were recorded for all samples. Silver layer sputtering and laser processing contributed to the appearance of additional peaks originating from Ag. Also, an F-derived signal was observable for samples I and II, which could be attributed to the fluoride-rich layer at the bottoms and walls of the fabricated nanotube structures [46]. Deposition of the chit/EE100 coating resulted in the appearance of additional peaks relating to carbon (C) and nitrogen (N) and a decrease in the intensity of peaks originating from the substrate material. Both laser treatment and electrophoretic deposition did not contaminate the samples with other elements.

The results of the corrosion tests are shown in Fig. 3 and Table 1. The OCP value (Table 1) was close to 0 V for all samples tested. According to the corrosion curves (Fig. 3a), the sample with the nanotube oxide layer (Sample I) showed the highest corrosion resistance (the lowest j$_{corr}$ value). The nanotube layer probably provided a tight ceramic barrier separating the metallic substrate from the SBF environment [47].
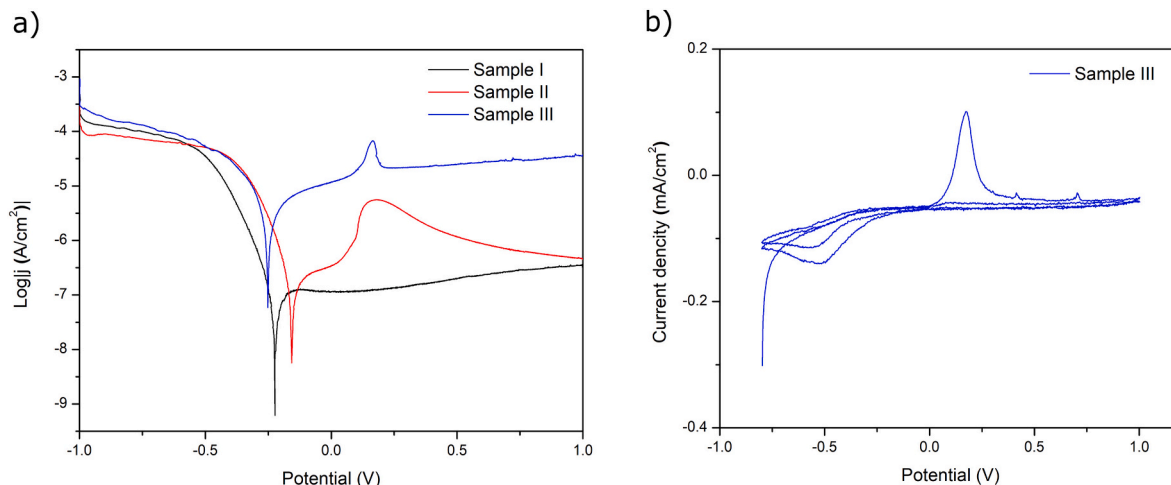
a)

b)

Fig. 3. (a) Corrosion curves of investigated samples, and (b) the linear voltammogram of the polymer-coated sample.

Table 1
The results of corrosion studies.

Sample	OCP (V)	E_{corr} (V)	j_{corr} (μA/cm^2)
I	−0.003	−0.224	0.122
II	0.007	−0.153	0.369
III	−0.031	−0.257	4.498

Further modifications (Sample II) resulted in the lowest corrosion resistance as the j_{corr} value was higher. The deep decrease in corrosion resistance of Sample III is most likely due to the appearance of an electrochemical cell composed of the polymer coating as an anode and oxide ceramic coating as a cathode, followed by localized fast corrosion. Fig. 3b shows linear voltammograms of sample III coated with chit/ EE100. The courses of curves overlap each other over in the whole measured range, except for the oxidation peak centered at 0.11 V. Its disappearance during consecutive runs indicates the complete dissolution of the polymer layer, and it supports the assumption of the creation of electrochemical cell, while the lack of additional features in the next scans shows the stability of the silver-modified surface underneath.

A representative graph of the frictional force vs. normal force relationship along with the microscopic scratch image obtained for a single scratch of the biopolymer coated sample is given in Fig. 4. Based on a sudden change of indenter friction force against the tested surface and scratch image, it was possible to determine the critical force (Lc) causing complete removal of biopolymer coating from the substrate, which allows quantification of the adhesion of the deposited coating. Based on all the results collected in Table 2, the average value of the Lc force from ten measurements was 41.97 ± 2.44 mN while the critical friction force (Lf) was 94.82 ± 6.10 mN. This value is in line with previous studies [35], although this is not a satisfactory result considering the invasive implant procedure. Implant coatings should have high adhesion to metallic substrates, especially under shear stress [48]. There is no other data in the literature regarding the mechanical properties of this type of biopolymer coatings.

The release characteristics of silver from silver-containing samples (samples II and III) after exposure to SBF solution with different pH values (7 and 3) at 39 °C for 1, 2, and 3 days are shown in Fig. 5. For a pH of 7 after 1 and 2 days of testing, the readings of the silver concentration in the SBF solution were below the limit of detection (LOD) or the limit of quantitation (LOQ), which for this study were 0.007 mg/L and 0.020 mg/L, respectively. Hence it can be assumed that after two days of testing the silver was practically not released. After three days of exposure, there was a noticeable increase in the silver concentration in solution, but for both samples, taking into account the measurement
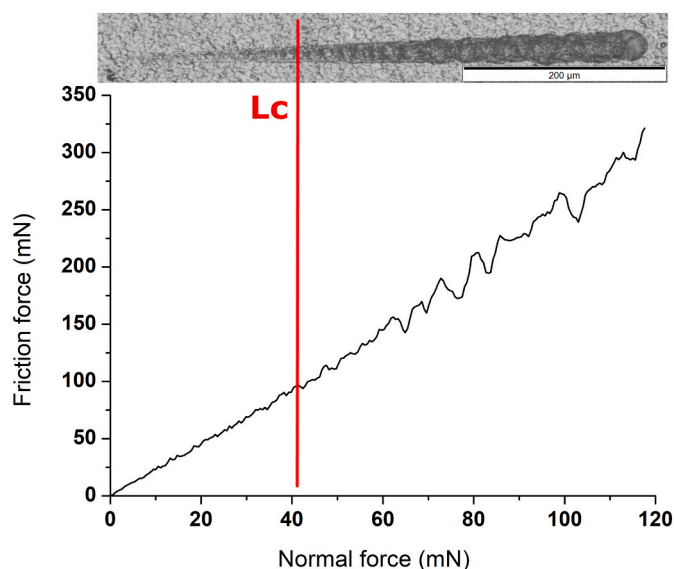

Fig. 4. Dependence of friction force versus normal force obtained for a single scratch during a scratch test with the critical force (Lc) marked, matched with a microscopic image of a scratch-made in a chit/EE100 coating.

Table 2
Results of critical frictional forces (Lf) and normal forces (Lc) obtained during individual scratches of chit/EE100 coatings.

Scratch number	Critical load, Lc (mN)	Critical friction, Lf (mN)
1	41.40	90.58
2	39.30	89.06
3	45.06	101.68
4	42.44	95.96
5	43.49	101.96
6	47.15	106.89
7	40.36	90.96
8	38.26	86.76
9	41.90	95.23
10	40.35	89.07

uncertainty, it remained at a similarly low level (approximately 0.06 mg/L). In the case of sample II, it is probably that the laser-generated silver nanoparticles are not all fused into the TiO$_2$ nanotube oxide layer matrix and due to poor adhesion, they detach from the substrate under the influence of the SBF solution flowing. Most likely, there was a
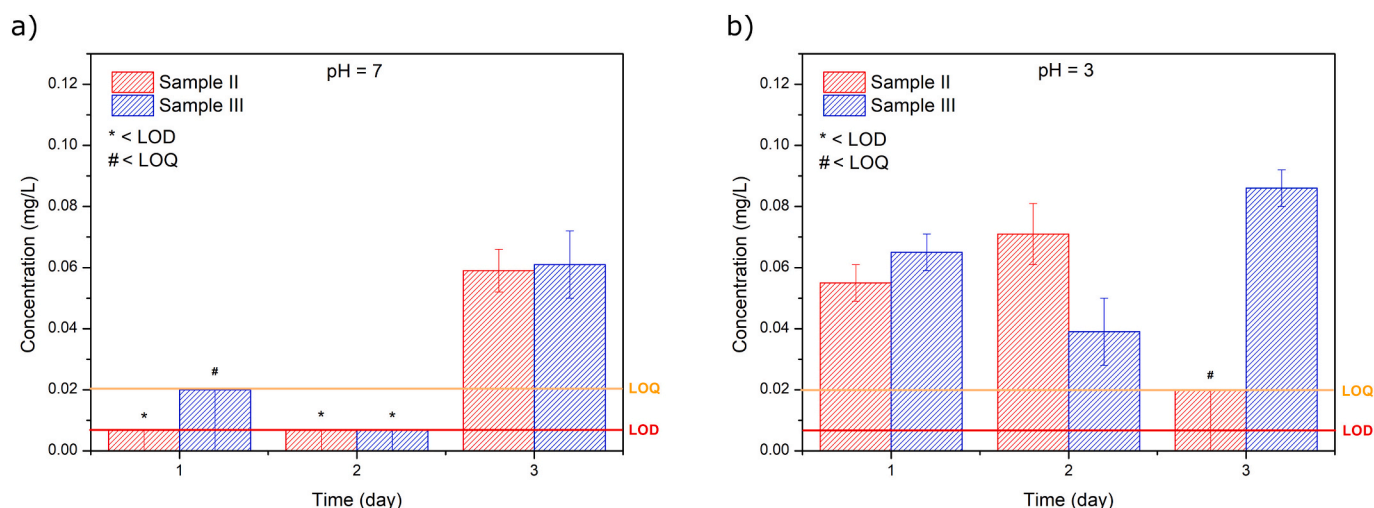
Fig. 5. Results of silver release into SBF solution from samples II and III immersed for 1, 2, and 3 days at two pH values of SBF solution: (a) pH = 7, (b) pH = 3.

loosely bound Ag layer on the modified TiO$_2$ surface that may have released during the first few days after sample II was placed in the pH-reduced SBF solution. Sample II released more silver at pH 3 than at pH 7 on Day 1 and Day 2, as the bare nanotube surface may be partially degraded in the acidic SBF environment. After Day 3, this process possibly stabilized and the release was inhibited. The biopolymer coating deposited on the modified nanotubes should contribute to a minimization of the silver amount released into the SBF fluid, but no such trend was observed. This may occur since the coating may have swelled upon exposure to SBF at elevated temperatures and thus some of the embedded nanoparticles managed to release [49]. It is therefore necessary to conduct long-term released studies on such structures. For a

pH of 3, an increase in the concentration of silver released into the SBF solution was observed after only 1st day, very soon compared to neutral pH. For the sample without biopolymer coating, there was a more pronounced increase in the concentration of released silver after two days of testing and a significant decrease below the LOQ after another day. The use of the chit/EE100 coating reduced then the release in the initial phase of the study, and after three days there has been severe degradation of the coating under the influence of the reduced pH associated with a notable release of silver [50]. Under the influence of an acidic pH environment, the protonation of the amino groups of chitosan and Eudragit E 100 is enhanced, so that the repulsive interaction between these groups causes the degradation of the biopolymer coating and the
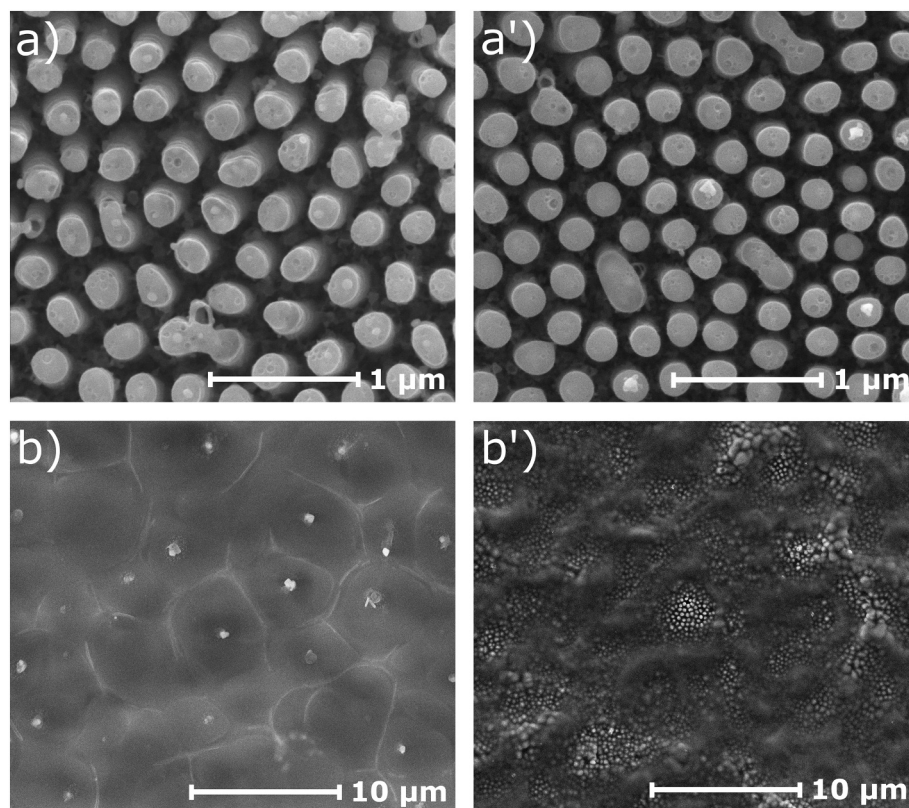
Fig. 6. Morphology: (a), (a') of the laser modified nanotube layer with fabricated AgNPs (Sample II); and (b), (b') of the chit/EE100 coating on a modified oxide nanotube layer (Sample III) after three days of immersion in the SBF solutions at different pH value: (a), (b) pH = 7; (a'), (b') pH = 3.

release of silver nanoparticles [51]. Previous studies [30] have demonstrated that complete degradation of the biopolymer coating occurs after 7 days of residence of chit/EE100-coated titanium samples in SBF solution at pH = 3. This was established based on the weight loss of the test samples. Hence, after three days of testing the silver release from the chit/EE100 coatings, partial dissolution had certainly occurred. A coated system would probably work better during the onset of local bacterial infection of the peri-implant tissues.

The morphology of the samples after testing the release of AgNPs into SBF solution at different pH is shown in Fig. 6. For sample II, for both pH values, the loss of silver nanoparticles from the encapsulated surfaces of TiO₂ nanotubes was evident. However, not all nanoparticles detached from the surface and were released into the SBF solution. The chit/EE100-coated sample had no apparent degradation after immersion in SBF at pH = 7. It probably became partially swollen during the test due to the absorption of the water contained in the SBF solution. Crystals of salts crystallized from the solution were visible on the coating. For acidic pH, areas of coating degradation and complete exposure of the modified nanoparticle substrate were visible.

To evaluate the antimicrobial properties of the samples the ASTM: E2149 method with slight modification was used, which is designed to measure the antimicrobial activity of non-leaching (non-water soluble) antimicrobial surfaces. The results of the antimicrobial activity tests are presented in the form of the degree of logarithmic reduction obtained after 24-h contact of *S. aureus* and *E. coli* inoculum with the tested materials (Fig. 7).

The obtained results show that the titania nanotubes do not exhibit any antimicrobial properties against *E. coli* and *S. aureus*. On the contrary, the number of microorganisms increased for Sample I which is illustrated by the bars in Fig. 7 with negative values. A decrease in bacterial growth of *E. coli* by 2.36 on a logarithmic scale (99.4%) was observed, however, for Sample II decorated with silver nanoparticles. The significant inhibition of the growth of *E. coli* by 3.58 on the logarithmic scale (99.99%) and a slight inhibition for *S. aureus* by 0.53 (77.5%) on the logarithmic scale occurred for sample III in the presence of silver nanoparticles and the chit/EE100 coating. Due to differences in the structure of the bacterial cell wall, which in the case of Gram-negative bacteria is narrower than that of Gram-positive bacteria, a differentiated effect of AgNPs on antimicrobial activity is observed. The thicker cell wall of Gram-positive bacteria limits their ability to take up silver nanoparticles in contrast to Gram-negative bacteria, which are susceptible to the antimicrobial activity of nanoparticles [52]. Also, chitosan has varying inhibition efficiencies against Gram-positive and Gram-negative bacteria [53]. Its antimicrobial activity is affected by physicochemical factors such as molecular weight, degree of deacetylation, pH, and changes due to modifications [54]. However, the main antimicrobial mechanism of chitosan and EE100 is due to its polycationic nature. Cell lysis caused by the electrostatic interaction between the positively charged polymer and the negatively charged cell membranes of microorganisms is greater the lower the pH of the environment. With a pKa in the range of 6.3–6.5, its antimicrobial activity decreases because pH is a key factor in the solubility of chitosan. However, Mania and *co*-workers proved that the antimicrobial activity of chitosan after appropriate modification of the polymer can also be maintained at a neutral pH [55]. It can be easily concluded that the antimicrobial activity against Gram-negative bacteria is the result of the layers containing silver nanoparticles and the chit/EE100 and that it is mainly due to the presence of the first component. On the other hand, only the layer containing chitosan inhibited the growth of Gram-positive bacteria. The test results indicated that in a neutral environment during 24 h (1 day) no release of silver ions into the SBF was observed, which does not mean that they have no effect on the bacterial inoculum. The inoculum was applied directly to the surface of the tested material, and the samples prepared in this way were incubated at a temperature suitable for the growth of microorganisms under the conditions of relative humidity of at least 50%. These are sufficient conditions for the growth of microorganisms in the absence of antimicrobial agents (control test) and for inhibition of their growth in the presence of such factors. The nanoparticle antimicrobial activity may be related to the release of metal ions, indirect action of reactive oxygen species, direct interaction between nanoparticles and microorganisms, immunostimulatory action or a result of several mechanisms mentioned above. The closest to presented results is the one concerning the direct contact of silver ions with cells that interact with their membrane proteins, changing the permeability of the cell wall membrane. Additionally, due to the negative charge of the cell walls of Gram-positive and Gram-negative bacteria, positively charged silver nanoparticles show greater antimicrobial efficacy than those with a negative charge [56].

4. Conclusions

Titanium dioxide nanotubes fabricated in a glycol-based electrolyte are vertically oriented, homogeneous, and separated.

Silver sputtering followed by laser irradiation of nanotubular titanium oxide layer originates in novel encapsulated nanotubes with formed AgNPs of about 30 nm in diameter. Laser radiation-induced melting of the nanotubes resulted in a decrease in nanotube length of about 30%.

The chit/EE100-based coating electrophoretically deposited on the laser-treated nanotube substrate exhibits relatively high uniformity and hydrophilicity (θ value about 65°). The average value of the critical force causing complete removal of the coating from the substrate was 41.97 ± 2.44 mN.

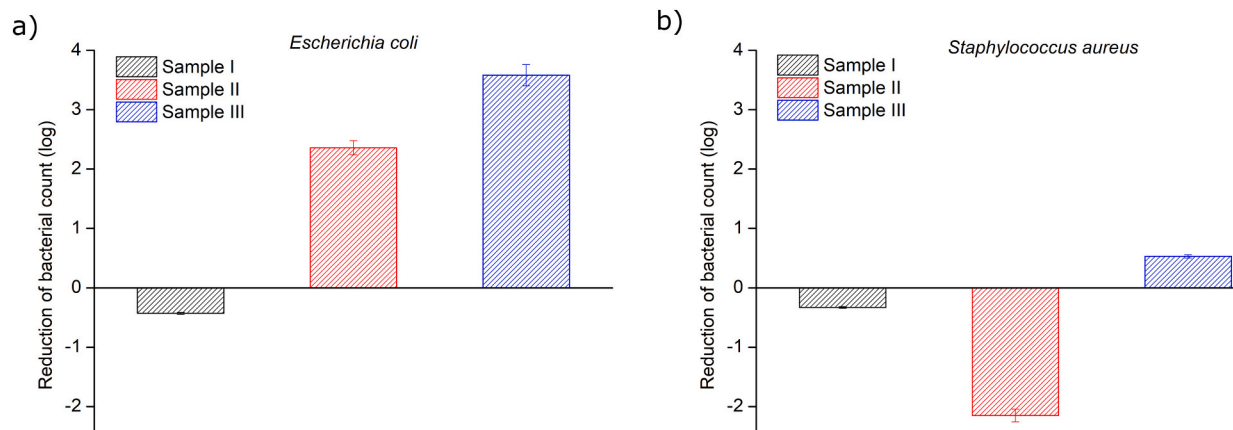Here proposed three-step modification of the titanium surface

Fig. 7. Comparison of the logarithmic reduction of bacteria cells number after incubation with samples I, II, and III for a) *Escherichia coli* and b) *Staphylococcus aureus*.

contributed to a satisfactory antimicrobial effect at the expense of corrosion resistance, but the recorded values of the corrosion potential for all the tested samples are of the order of $\mu A/cm^2$ which indicates the high corrosion resistance of all the samples. SEM studies of the samples after the release of AgNPs into SBF solution revealed that for neutral pH the chit/EE100 coating was present on the surface, it undergoes partial swelling in SBF solution and dissolves under acidic pH. Long-term AgNPs release studies are needed to accurately determine the mechanism and timing of AgNPs release. Previous studies have shown that the addition of Eudragit to chitosan coatings improves the stability of these coatings in SBF. Perhaps a greater addition of EE100 to the chitosan suspension would improve the release kinetics of AgNPs into SBF solution at different pH.

CRediT authorship contribution statement

Łukasz Pawłowski: Conceptualization, Methodology, Validation, Formal analysis, Investigation, Data curation, Writing – original draft, Writing – review & editing, Visualization. **Jakub Wawrzyniak:** Conceptualization, Methodology, Validation, Formal analysis, Investigation, Data curation, Writing – original draft, Writing – review & editing, Visualization. **Adrianna Banach-Kopeć:** Methodology, Investigation, Writing – review & editing. **Bartłomiej Michał Cieślik:** Methodology, Investigation, Writing – review & editing. **Kacper Jurak:** Methodology, Investigation, Writing – review & editing. **Jakub Karczewski:** Investigation. **Robert Tylingo:** Writing – review & editing, Supervision. **Katarzyna Siuzdak:** Writing – review & editing, Supervision. **Andrzej Zieliński:** Writing – review & editing, Supervision.

Declaration of competing interest

The authors declare that they have no known competing financial interests or personal relationships that could have appeared to influence the work reported in this paper.

Acknowledgments

References

[1] A. Kurup, P. Dhatrak, N. Khasnis, Surface modification techniques of titanium and titanium alloys for biomedical dental applications: a review, Mater. Today Proc. 39 (2021) 84–90, https://doi.org/10.1016/J.MATPR.2020.06.163.

[2] A. Barfeie, J. Wilson, J. Rees, Implant surface characteristics and their effect on osseointegration, Br. Dent. J. 2185 (218) (2015) E9, https://doi.org/10.1038/sj.bdj.2015.171.

[3] Z. Lockman, S. Sreekantan, S. Ismail, L. Schmidt-Mende, J.L. MacManus-Driscoll, Influence of anodisation voltage on the dimension of titania nanotubes, J. Alloys Compd. 503 (2010) 359–364, https://doi.org/10.1016/J.JALLCOM.2009.12.093.

[4] D. Losic, M.S. Aw, A. Santos, K. Gulati, M. Bariana, Titania nanotube arrays for local drug delivery: recent advances and perspectives, Expert Opin. Drug Deliv. 12 (2015) 103–127, https://doi.org/10.1517/17425247.2014.945418.

[5] K. Wang, H. Jin, Q. Song, J. Huo, J. Zhang, P. Li, Titanium dioxide nanotubes as drug carriers for infection control and osteogenesis of bone implants, Drug Deliv. Transl. Res. 11 (2021) 1456–1474, https://doi.org/10.1007/s13346-021-00980-z.

[6] S.Y. Im, K.M. Kim, J.S. Kwon, Antibacterial and osteogenic activity of titania nanotubes modified with electrospray-deposited tetracycline nanoparticles, Nanomaterials. 10 (2020), https://doi.org/10.3390/nano10061093.

[7] S.D. Puckett, E. Taylor, T. Raimondo, T.J. Webster, The relationship between the nanostructure of titanium surfaces and bacterial attachment, Biomaterials 31 (2010) 706–713, https://doi.org/10.1016/J.BIOMATERIALS.2009.09.081.

[8] K. Gulati, S. Ramakrishnan, M.S. Aw, G.J. Atkins, D.M. Findlay, D. Losic, Biocompatible polymer coating of titania nanotube arrays for improved drug elution and osteoblast adhesion, Acta Biomater. 8 (2012) 449–456, https://doi.org/10.1016/j.actbio.2011.09.004.

[9] P. Liu, Y. Hao, Y. Zhao, Z. Yuan, Y. Ding, K. Cai, Surface modification of titanium substrates for enhanced osteogenetic and antibacterial properties, Colloids Surf. B Biointerfaces 160 (2017) 110–116, https://doi.org/10.1016/j.colsurfb.2017.08.044.

[10] Z. Riahi, S.A. Seyedkhani, S.K. Sadrnezhaad, Electrophoretic encapsulation for slow release of vancomycin from perpendicular TiO2 nanotubes grown on Ti6Al4V electrodes, Mater. Res. Express. 6 (2019), https://doi.org/10.1088/2053-1591/ab6c98.

[11] J. Zhou, M.A. Frank, Y. Yang, A.R. Boccaccini, S. Virtanen, A novel local drug delivery system: superhydrophobic titanium oxide nanotube arrays serve as the drug reservoir and ultrasonication functions as the drug release trigger, Mater. Sci. Eng. C. 82 (2018) 277–283, https://doi.org/10.1016/j.msec.2017.08.066.

[12] T. Li, N. Wang, S. Chen, R. Lu, H. Li, Z. Zhang, Antibacterial activity and cytocompatibility of an implant coating consisting of TiO2 nanotubes combined with a GL13K antimicrobial peptide, Int. J. Nanomedicine 12 (2017) 2995–3007, https://doi.org/10.2147/IJN.S128775.

[13] A.N. Coman, A. Mare, C. Tanase, E. Bud, A. Rusu, Silver-deposited nanoparticles on the titanium nanotubes surface as a promising antibacterial material into implants, Metals (Basel) 11 (2021) 1–16, https://doi.org/10.3390/met11010092.

[14] M. Nycz, K. Arkusz, D.G. Pijanowska, Influence of the silver nanoparticles (AgNPs) formation conditions onto titanium dioxide (TiO2) nanotubes based electrodes on their impedimetric response, Nanomaterials. 9 (2019), https://doi.org/10.3390/nano9081072.

[15] R. Zia, M. Riaz, N. Farooq, A. Qamar, S. Anjum, Antibacterial activity of ag and cu nanoparticles synthesized by chemical reduction method: a comparative analysis, Mater. Res. Express. 5 (2018), 075012, https://doi.org/10.1088/2053-1591/aacf70.

[16] F. Ordikhani, A. Simchi, Long-term antibiotic delivery by chitosan-based composite coatings with bone regenerative potential, Appl. Surf. Sci. 317 (2014) 56–66, https://doi.org/10.1016/j.apsusc.2014.07.197.

[17] B. Tyliszczak, A. Drabczyk, S. Kudłacik-Kramarczyk, K. Bialik-Wąs, R. Kijkowska, A. Sobczak-Kupiec, Preparation and cytotoxicity of chitosan-based hydrogels modified with silver nanoparticles, Colloids Surf. B Biointerfaces. 160 (2017) 325–330, https://doi.org/10.1016/j.colsurfb.2017.09.044.

[18] R. Socrates, O. Prymak, K. Loza, N. Sakthivel, A. Rajaram, M. Epple, S. Narayana Kalkura, Biomimetic fabrication of mineralized composite films of nanosilver loaded native fibrillar collagen and chitosan, Mater. Sci. Eng. C Mater. Biol. Appl. 99 (2019) 357–366, https://doi.org/10.1016/J.MSEC.2019.01.101.

[19] N.T.P. Nguyen, L.V.H. Nguyen, N.T. Thanh, V. Van Toi, T. Ngoc Quyen, P.A. Tran, H.M. David Wang, T.H. Nguyen, Stabilization of silver nanoparticles in chitosan and gelatin hydrogel and its applications, Mater. Lett. 248 (2019) 241–245, https://doi.org/10.1016/J.MATLET.2019.03.103.

[20] L. Ren, Y. Zhao, L. Yang, W. Cao, H. Wang, X. Lian, X. Gao, B. Niu, W. Li, Preparation and characterization of the catechol functionalized chitosan-Ag NPs deposited onto titanium surface, Surf. Coat. Technol. 420 (2021), 127319, https://doi.org/10.1016/J.SURFCOAT.2021.127319.

[21] Ł. Pawłowski, M. Bartmański, A. Mielewczyk-Gryń, B.M. Cieślik, G. Gajowiec, A. Zieliński, Electrophoretically deposited Chitosan/Eudragit E 100/AgNPs composite coatings on titanium substrate as a silver release system, Materials (Basel). 14 (2021) 4533, https://doi.org/10.3390/ma14164533.

[22] A.K. Mishra, J. Lim, J. Lee, S. Park, Y. Seo, H. Hwang, J.K. Kim, Control drug release behavior by highly stable and pH sensitive poly(N-vinylpyrrolidone)-block-poly(4-vinylpyridine) copolymer micelles, Polymer (Guildf). 213 (2021), 123329, https://doi.org/10.1016/J.POLYMER.2020.123329.

[23] M. Atif, C. Chen, M. Irfan, F. Mumtaz, K. He, M. Zhang, L. Chen, Y. Wang, Poly(2-methyl-2-oxazoline) and poly(4-vinyl pyridine) based mixed brushes with switchable ability toward protein adsorption, Eur. Polym. J. 120 (2019), 109199, https://doi.org/10.1016/J.EURPOLYMJ.2019.08.026.

[24] A. Alshhab, E. Yilmaz, Sodium alginate/poly(4-vinylpyridine) polyelectrolyte multilayer films: preparation, characterization and ciprofloxacin HCl release, Int. J. Biol. Macromol. 147 (2020) 809–820, https://doi.org/10.1016/J.IJBIOMAC.2019.10.058.

[25] I.G. Simões, A.C. dos Reis, M.L. da Costa Valente, Analysis of the influence of surface treatment by high-power laser irradiation on the surface properties of titanium dental implants: a systematic review, J. Prosthet. Dent. (2021) 1–8, https://doi.org/10.1016/j.prosdent.2021.07.026.

[26] K. Katahira, A. Ezura, K. Ohkawa, J. Komotori, H. Ohmori, Generation of bio-compatible titanium alloy surfaces by laser-induced wet treatment, CIRP Ann. - Manuf. Technol. 65 (2016) 237–240, https://doi.org/10.1016/j.cirp.2016.04.053.

[27] B.F. Mohazzab, B. Jaleh, A. Fattah-alhosseini, F. Mahmoudi, A. Momeni, Laser surface treatment of pure titanium: microstructural analysis, wear properties, and corrosion behavior of titanium carbide coatings in Hank's physiological solution, Surfaces and Interfaces. 20 (2020), 100597, https://doi.org/10.1016/j.surfin.2020.100597.

[28] M. Bahiraei, Y. Mazaheri, M. Sheikhi, A. Heidarpour, Mechanism of TiC formation in laser surface treatment of the commercial pure titanium pre-coated by carbon using PVD process, J. Alloys Compd. 834 (2020), 155080, https://doi.org/10.1016/j.jallcom.2020.155080.

[29] J. Lu, T. Huang, Z. Liu, X. Zhang, R. Xiao, Long-term wettability of titanium surfaces by combined femtosecond laser micro/nano structuring and chemical treatments, Appl. Surf. Sci. 459 (2018) 257–262, https://doi.org/10.1016/j.apsusc.2018.08.004.

[30] Ł. Pawłowski, M. Bartmański, G. Strugała, A. Mielewczyk-Gryń, M. Jażdżewska, A. Zieliński, Electrophoretic deposition and characterization of Chitosan/Eudragit E 100 coatings on titanium substrate, Coatings 10 (2020) 607, https://doi.org/10.3390/coatings10070607.

[31] J. Wawrzyniak, K. Grochowska, J. Karczewski, P. Kupracz, J. Ryl, A. Dołęga, K. Siuzdak, The geometry of free-standing titania nanotubes as a critical factor controlling their optical and photoelectrochemical performance, Surf. Coatings Technol. 389 (2020), https://doi.org/10.1016/j.surfcoat.2020.125628.

[32] C.I. Dias, J.F. Mano, N.M. Alves, PH-responsive biomineralization onto chitosan grafted biodegradable substrates, J. Mater. Chem. 18 (2008) 2493–2499, https://doi.org/10.1039/b800776d.

[33] B. Świeczko-Żurek, M. Bartmański, Investigations of titanium implants covered with hydroxyapatite layer, Adv. Mater. Sci. 16 (2016), https://doi.org/10.1515/adms-2016-0011.

[34] K.A. Gross, M. Babovic, Influence of abrasion on the surface characteristics of thermally sprayed hydroxyapatitae coatings, Biomaterials 23 (2002) 4731–4737, https://doi.org/10.1016/S0142-9612(02)00222-3.

[35] Ł. Pawłowski, M. Bartmański, A. Mielewczyk-Gryń, A. Zieliński, Effects of surface pretreatment of titanium substrates on properties of electrophoretically deposited biopolymer chitosan/eudragit e 100 coatings, Coatings 11 (2021), https://doi.org/10.3390/coatings11091120.

[36] L. Cordero-Arias, S. Cabanas-Polo, H. Gao, J. Gilabert, E. Sanchez, J.A. Roether, D.W. Schubert, S. Virtanen, A.R. Boccaccini, Electrophoretic deposition of nanostructured-TiO2/chitosan composite coatings on stainless steel, RSC Adv. 3 (2013) 11247–11254, https://doi.org/10.1039/c3ra40535d.

[37] S. Kasraei, M. Azarsina, Addition of silver nanoparticles reduces the wettability of methacrylate and silorane-based composites, Braz. Oral Res. 26 (2012) 505–510, https://doi.org/10.1590/S1806-83242012000600004.

[38] V. Linares, C.J. Yarce, J.D. Echeverri, E. Galeano, C.H. Salamanca, Relationship between degree of polymeric ionisation and hydrolytic degradation of Eudragit® E polymers under extreme acid conditions, Polymers (Basel). 11 (2019), https://doi.org/10.3390/polym11061010.

[39] G.B. Hoflund, J.F. Weaver, W.S. Epling, Ag Foil by XPS (2021), https://doi.org/10.1116/1.1247777.

[40] G.B. Hoflund, J.F. Weaver, W.S. Epling, AgO XPS spectra, Surf. Sci. Spectra. 3 (2021) 163, https://doi.org/10.1116/1.1247779.

[41] W.L. Wiese, D.C. Morton, P.S. Lee, D. Mangelinck, K.L. Pey, Y. Yee Li, S.V. Calderon, R. Escobar Galindo, N. Benito, C. Palacio, A. Cavaleiro, S. Carvalho, Ag+ release inhibition from ZrCN–Ag coatings by surface agglomeration mechanism: structural characterization, J. Phys. D Appl. Phys. 46 (2013), 325303, https://doi.org/10.1088/0022-3727/46/32/325303.

[42] X. Chen, S.S. Mao, Titanium dioxide nanomaterials: synthesis, properties, modifications, and applications, Chem. Rev. 107 (2007) 2891–2959, https://doi.org/10.1021/CR0500535.

[43] N. Joshi, N. Jain, A. Pathak, J. Singh, R. Prasad, C.P. Upadhyaya, Biosynthesis of silver nanoparticles using Carissa carandas berries and its potential antibacterial activities, J. Sol-Gel Sci. Technol. 86 (2018) 682–689, https://doi.org/10.1007/S10971-018-4666-2/FIGURES/5.

[44] J.M. McLellan, A. Siekkinen, J. Chen, Y. Xia, Comparison of the surface-enhanced raman scattering on sharp and truncated silver nanocubes, Chem. Phys. Lett. 427 (2006) 122–126, https://doi.org/10.1016/J.CPLETT.2006.05.111.

[45] C.-M. Chuang, M.-C. Wu, W.-F. Su, K.-C. Cheng, Y.-F. Chen, High intensity fluorescence of photoactivated silver oxide from composite thin film with periodic array structure, Appl. Phys. Lett. 89 (2006), 061912, https://doi.org/10.1063/1.2222252.

[46] F. Riboni, N.T. Nguyen, S. So, P. Schmuki, Aligned metal oxide nanotube arrays: key-aspects of anodic TiO2 nanotube formation and properties, Nanoscale Horiz. 1 (2016) 445–466, https://doi.org/10.1039/C6NH00054A.

[47] S. Wu, S. Wang, W. Liu, X. Yu, G. Wang, Z. Chang, D. Wen, Microstructure and properties of TiO2 nanotube coatings on bone plate surface fabrication by anodic oxidation, Surf. Coat. Technol. 374 (2019) 362–373, https://doi.org/10.1016/j.surfcoat.2019.06.019.

[48] U. Brohede, S. Zhao, F. Lindberg, A. Mihranyan, J. Forsgren, M. Strømme, H. Engqvist, A novel graded bioactive high adhesion implant coating, Appl. Surf. Sci. 255 (2009) 7723–7728, https://doi.org/10.1016/j.apsusc.2009.04.149.

[49] S. Bagherifard, Mediating bone regeneration by means of drug eluting implants: from passive to smart strategies, Mater. Sci. Eng. C. 71 (2017) 1241–1252, https://doi.org/10.1016/j.msec.2016.11.011.

[50] V. Boeris, D. Romanini, B. Farruggia, G. Picó, Interaction and complex formation between catalase and cationic polyelectrolytes: chitosan and eudragit E100, Int. J. Biol. Macromol. 45 (2009) 103–108, https://doi.org/10.1016/j.ijbiomac.2009.04.009.

[51] Ł. Pawłowski, pH-dependent composite coatings for controlled drug delivery system - review, Inżynieria Mater. 1 (2019) 4–9, https://doi.org/10.15199/28.2019.3.1.

[52] I.X. Yin, J. Zhang, I.S. Zhao, M.L. Mei, Q. Li, C.H. Chu, The antibacterial mechanism of silver nanoparticles and its application in Dentistry, Int. J. Nanomedicine 15 (2020) 2555–2562, https://doi.org/10.2147/IJN.S246764.

[53] H. Yilmaz Atay, Antibacterial activity of chitosan-based systems, Funct. Chitosan (2020) 457, https://doi.org/10.1007/978-981-15-0263-7_15.

[54] S. Mania, K. Partyka, J. Pilch, E. Augustin, M. Cieślik, J. Ryl, J.R. Jinn, Y.J. Wang, A. Michałowska, R. Tylingo, Obtaining and characterization of the PLA/chitosan foams with antimicrobial properties achieved by the emulsification combined with the dissolution of chitosan by CO2 saturation, Mol 24 (2019) 4532, https://doi.org/10.3390/MOLECULES24244532.

[55] S. Mania, R. Tylingo, E. Augustin, K. Gucwa, J. Szwacki, H. Staroszczyk, Investigation of an elutable N-propylphosphonic acid chitosan derivative composition with a chitosan matrix prepared from carbonic acid solution, Carbohydr. Polym. 179 (2018) 196–206, https://doi.org/10.1016/J.CARBPOL.2017.09.082.

[56] X. Fan, L. Yahia, E. Sacher, Antimicrobial properties of the Ag, Cu nanoparticle system, Biology 10 (2) (2021) 137, https://doi.org/10.3390/biology10020137.